Helical conducting edge states in narrow-gap semiconductors without band inversion

Wen-Kai Lou [1,2] Wen Yang,[3,*] and Kai Chang[1,2,4,†]

[1]*SKLSM, Institute of Semiconductors, Chinese Academy of Sciences, P.O. Box 912, Beijing 100083, China*

[2]*College of Materials Science and Opto-electronic Technology, Center of Materials Science and Optoelectronics Engineering, University of Chinese Academy of Sciences, Beijing 100049, China*

[3]*Beijing Computational Science Research Center, Beijing 100193, China*

[4]*Beijing Academy of Quantum Information Sciences, Beijing 100193, China*

(Received 4 October 2021; accepted 30 December 2021; published 18 January 2022)

Band inversion accompanied by the emergence of gapless and helical edge states at the boundary is a hallmark of 2D topological insulators. However, a recent experiment reports the existence of edge states before band inversion in InAs/GaSb quantum wells [F. Nichele *et al.*, New J. Phys. **18**, 083005 (2016)]. The underlying physics remains an open problem. Here we provide a possible solution by showing that helical edge states emerge before band inversion as long as the bulk gap falls below a *positive* threshold determined by the particle-hole asymmetry and interband coupling. In the presence of quantum confinement or local electrostatic potential near the boundary, these edge states may enter the gap of bulk states and be detected as edge conductance in transport measurements. Our work reveals the possible existence of the helical conducting edge states in a large class of narrow-gap semiconductors.

DOI: 10.1103/PhysRevB.105.045305

Introduction. Topological insulators (TIs) are new states of quantum matter caused by the inversion of the energy bands [1–13]. Ever since the discovery of two-dimensional TIs, the existence of gapless edge states and the resulting quantized edge conductance have been widely used as a fingerprint for their experimental detection. Two paradigmatic examples are the theoretical prediction [5,8] and experimental verification [6,9] of HgTe and InAs/GaSb quantum wells as two-dimensional TIs**.** However, recent experiments show that the edge states appear before the band inversion in InAs/GaSb quantum wells and even survive under a perpendicular magnetic field [14]. The physics underlying this controversy remains a challenge [14–28] .

In this work we demonstrate theoretically that helical edge states emerge before band inversion once the bulk gap drops below a *positive* threshold determined by the degree of particle-hole asymmetry and the strength of the interband coupling. Based on the $\mathbf{k}\cdot\mathbf{p}$ theory [29], we derive analytical criterion for the existence of these nontopological edge states in the normal insulator (NI) phase and construct a full phase diagram showing that the nontopological edge states in the NI phase evolve *smoothly* across the phase boundary into the topological edge states in the TI phase. This finding identifies the particle-hole asymmetry and the interband coupling as crucial ingredients giving rise to conducting helical edge states without band inversion and reveals the possible existence of the helical conducting edge states in a large class of narrow-gap semiconductors. Moreover, these nontopological edge states may be driven into the gap of the bulk states by either quantum confinement effect or local electrostatic potential near the edges (either due to unintended potential fluctuation or by utilizing the side-gate technique [30–33]) and become detectable by transport measurements [6,9,34–38]. Since unintended potential fluctuation is ubiquitous in electrically gated samples, our work also provides a possible solution to the puzzling observation of edge-state conductance in the NI phase of InAs/GaSb quantum wells [14,16].

Helical edge states in NI phase. The four-band Bernevig-Hughes-Zhang (BHZ) model [5] captures the crucial features of the low-energy physics of narrow-gap semiconductors (see Appendix for comparison with the eight-band Kane model). For 2D semiconductors lying in the xy plane, the BHZ Hamiltonian consists of a 2×2 spin-up block under the basis $|E,\uparrow\rangle, |HH,\uparrow\rangle$ and a 2×2 spin-down block under the basis $|E,\downarrow\rangle = \mathcal{T}|E,\uparrow\rangle$ and $|HH,\downarrow\rangle = \mathcal{T}|HH,\uparrow\rangle$ connected by time reversal $\mathcal{T}$. The energy spectrum and eigenstates of the spin-down block are obtained from those of the spin-up block by time reversal, so we only consider the spin-up block:

$$H = \begin{bmatrix} M + B_+\left(\hat{k}_x^2 + \hat{k}_y^2\right) & A(\hat{k}_x + i\hat{k}_y) \\ A(\hat{k}_x - i\hat{k}_y) & -M - B_-\left(\hat{k}_x^2 + \hat{k}_y^2\right) \end{bmatrix}, \quad (1)$$

where $\hat{\mathbf{k}} \equiv -i\nabla$ is the momentum operator and $B_\pm \equiv B \pm D$. Here the sign of B and D are opposite to the conventional choice [2], so that $MB > 0$ corresponds to the NI phase and $MB < 0$ corresponds to the TI phase. When $D = 0$, the BHZ Hamiltonian Eq. (1) has particle-hole symmetry (also known as charge conjugation symmetry) $\mathcal{C}H\mathcal{C}^{-1} = -H$, where $\mathcal{C} \equiv \mathcal{T}C$ is antiunitary and $C = |E\rangle\langle HH| + \text{H.c.}$ is unitary. Previous studies on the edge states in the BHZ model [2] focused on some special regimes of the parameters and found edge states in the TI phase only [10,11]. Here we are going to develop an analytical description for edge states over the full range of parameters.

*wenyang@csrc.ac.cn

†kchang@semi.ac.cn

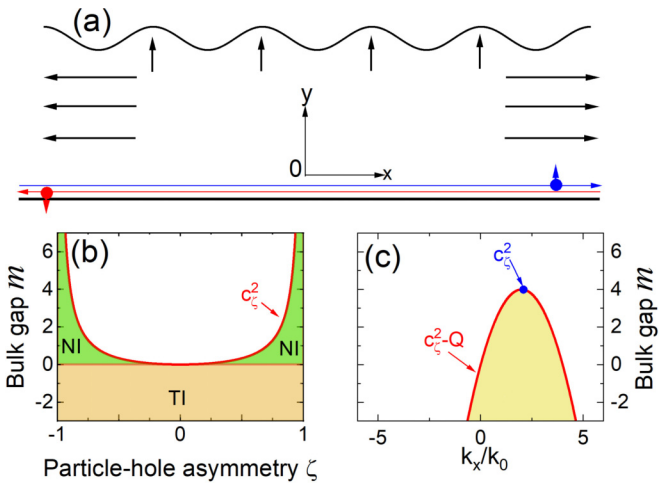

FIG. 1. Helical edge states in the normal insulator (NI) phase of the BHZ model on a half-space $y > 0$ of the xy plane. (a) Sketch of the helical edge states with spin-velocity locking. (b) Phase diagram in the $m - \zeta$ plane for the appearance of edge states. The dimensionless variable $m \equiv 4MB/A^2$ measures the ratio between the bulk gap $2M$ and the interband coupling, while $\zeta \equiv D/B$ or $c_\zeta \equiv \zeta/\sqrt{1-\zeta^2}$ quantifies the degree of particle-hole asymmetry. (c) Momentum window in the $m - k_x$ plane for the appearance of spin-up edge states. Its mirror reflection about $k_x = 0$ gives the momentum window for the spin-down edge states. Here $Q \equiv (k_x/k_0 - c_\zeta)^2$ and we take $c_\zeta = 2$.

As shown in Fig. 1(a), we consider spin-up electrons moving inside a semi-infinite plane $y \geqslant 0$ and take the trial wave function $\psi(x, y) = e^{ik_x x}\psi(y)$, where $k_x \in \mathbb{R}$. To solve the Schrödinger equation $H\psi(y) = E\psi(y)$ along the y axis subjected to the hard-wall boundary condition at $y = 0$, we use the standard mode-matching method. The key steps are as follows (see the Supplemental Material for more details [39]). The first step is to find the general solutions without any boundary conditions. Given the energy E, using the trial wave function $\psi(y) = [\alpha, \beta]^T e^{-\kappa y}$, the secular equation gives four solutions for κ, as denoted by $\kappa_\pm$ and $-\kappa_\pm$. For a certain range of the parameters and certain range of the energy E, the solutions have nonzero real parts. We are interested in this regime, since it corresponds to the existence of edge states localized near the boundary $y = 0$. In this case we choose $\kappa_\pm$ to have positive real parts. Among the four solutions, only the two wave functions [as denoted by $\psi_\pm(y)$] associated with the solutions $\kappa_\pm$ are physical, i.e., finite at $y \to +\infty$. The general solution is their linear combination: $\psi(y) = c_+\psi_+(y) + c_-\psi_-(y)$. Imposing the hard-wall boundary condition $\psi(y = 0) = 0$ determines the allowed energy

$$E(k_x) = -\zeta M - 2B\sqrt{1-\zeta^2}k_0 k_x \tag{2}$$

and the wave function $\psi(y) \propto e^{-\kappa_+ y} - e^{-\kappa_- y}$ characterized by the decay exponents

$$\kappa_\pm = k_0\sqrt{c_\zeta^2 + 1} \pm k_0\sqrt{Q + m + 1}, \tag{3}$$

where $k_0 \equiv |A|/(2|B|)$, $\zeta \equiv D/B$, or $c_\zeta \equiv \zeta/\sqrt{1-\zeta^2}$ quantifies the degree of particle-hole asymmetry, $Q \equiv (k_x/k_0 - c_\zeta)^2$, and the dimensionless ratio $m \equiv 4MB/A^2$ between the bulk gap $2M$ and the interband coupling separates the NI phase $m > 0$ and the TI phase $m < 0$.

TABLE I. Threshold bulk gap for the appearance of edge states in typical semiconductor quantum wells: CdTe/HgTe/CdTe, CdTe/InSb/CdTe, AlSb/InAs/AlSb, AlSb/GaSb/AlSb, AlAs/GaAs/AlAs, InP/$In_{0.53}Ga_{0.47}As$/InP. (See the online Supplemental Materials for details about the calculation [39]. The bulk eight-band Kane Hamiltonian and corresponding parameters and the Löwdin perturbation theory are demonstrated in [39]; see, also, Refs. [5,11,40–45] therein.)

Quantum well	HgTe	InSb	InAs	GaSb	GaAs	InGaAs
Threshold gap (meV)	121.8	45.8	208.8	163.5	160.5	192.9

Since edge states require $\mathrm{Re}(\kappa_\pm) > 0$ or equivalently $c_\zeta^2 + 1 > 0$ and $c_\zeta^2 > m + Q$, the condition for the emergence of edge states is [see Fig. 1(b)]

$$m < c_\zeta^2 \quad (\text{for } \zeta^2 < 1). \tag{4}$$

Under this condition, edge states emerge inside a momentum window centered at c_ζ [see Fig. 1(c)]:

$$\left|\frac{k_x}{k_0} - c_\zeta\right| < \sqrt{c_\zeta^2 - m}. \tag{5}$$

This identifies the interband coupling A and the particle-hole asymmetry ζ or c_ζ, in addition to the bulk gap $2M$, as crucial ingredients giving rise to edge states. The seminal work by König *et al.* [11] considered the particle-hole symmetric regime $\zeta = c_\zeta = 0$, so they found edge states in the TI phase only. By contrast, our work reveals that when the particle-hole symmetry is broken, edge states also emerge in the highest valence band (for $\zeta > 0$) or the lowest conduction band (for $\zeta < 0$) of the NI phase [see Fig. 1(b)]. When $-1 < m < 0$, all edge states exhibit biexponential decay $\psi(y) \propto e^{-\kappa_+ y} - e^{-\kappa_- y}$; when $m < -1$, those edge states lying in the narrower momentum window $|k_x/k_0 - c_\zeta| < \sqrt{-1-m}$ exhibit exponential decay $\psi(y) \propto e^{-y\,\mathrm{Re}(\kappa_+)}$. In other words, the NI phase supports biexponential edge states, while the TI phase supports both biexponential and exponential edge states. Since the vast majority of realistic semiconductor systems have no particle-hole symmetry, edge states are expected in these systems as long as the bulk gap $2M$ is made sufficiently small. In Table I we list the threshold bulk gap for the appearance of edge states in typical semiconductor quantum wells [11,46–56] .

Without loss of generality, we consider a 200-nm-wide quantum spin Hall bar (QSHB) made from HgTe quantum well [see Fig. 2(a)] and calculate its energy spectrum by exact numerical diagonalization using the parameters $A = 365$ meV nm, $B = 686$ meV nm^2, and $D = 512$ meV nm^2 from Ref. [11], and $M = +40$ meV, corresponding to the NI phase with broken particle-hole symmetry $\zeta \approx 0.75$ and $c_\zeta \approx 1.1$. Since the QSHB is wide, our analytical results can well describe the edge states at the lower boundary of the QSHB, while $k_x \to -k_x$ describes the edge states at the upper boundary. Since the particle-hole asymmetry $\zeta \approx 0.75$ is positive, our analytical results predict that the lower (upper) boundary of the QSHB supports edge states inside the momentum

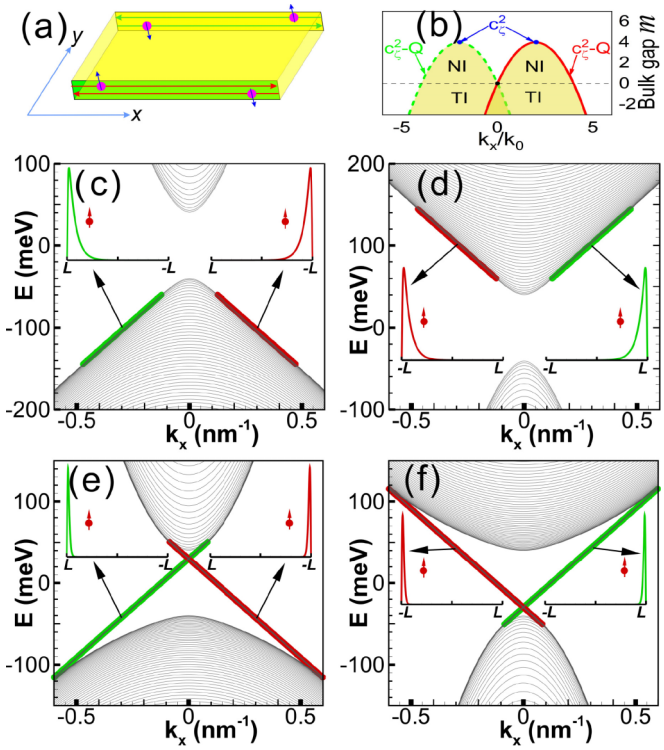

FIG. 2. (a) Sketch of the helical edge states in the NI phase of the QSHB structure. (b) Momentum windows for the appearance of spin-up edge states in the lower (red line) and upper (green line) edges of the QSHB, with $c_\zeta = 2$. (c, d) Energy spectra for a 200-nm-wide QSHB in the NI phase $M = 40$ meV with $D = 512$ meV nm^2 [for (c)] or $D = -512$ meV nm^2 [for (d)]: gray lines for exact numerical results for all the energy bands, thick red (green) line segments for our analytical results for the momentum window and energy dispersion of edge states at the lower (upper) boundary of the QSHB. The insets show the electron density distribution for typical edge states. (e) [(f)] is the same as (c) [(d)] except that $M = -40$ meV.

window Eq. (5) [Eq. (5) with $k_x \to -k_x$] of the highest valence band. This is confirmed by Fig. 2(c): inside these momentum windows, the numerically calculated energy dispersion of the highest valence band agree well with the analytical edge-state dispersion Eq. (2), and the corresponding electron density distributions [see the inset of Fig. 2(c)] indeed localize at the boundary of the QSHB. The detailed transition from bulk states (localized near the center of the QSHB) to edge states (localized at the boundary) when k_x enters the edge-state window and the transition from edge states back to bulk states once k_x goes out of the edge-state window can be found in the Supplemental Material [39]. When the sign of D is reversed, ζ also changes sign, then the edge states go to the lowest conduction band [see Fig. 2(d)], in agreement with our analytical results.

The analytical expressions Eqs. (2)–(5) not only predict the emergence of edge states in the NI phase but also offer another perspective to understand the origin of the topological edge states in the TI phase. Suppose we start from a wide-gap NI phase and continuously decrease the ratio m between the bulk gap $2M$ and the interband coupling, keeping other parameters fixed. As shown in Fig. 2(b), when m drops below c_ζ^2, the lower (upper) boundary of the QSHB begins to support edge states inside the momentum window Eq. (5) [Eq. (5) with $k_x \to -k_x$], whose width increases with the successive decrease of m. When m decreases to zero, the bulk gap closes and the edge-state momentum windows for the upper and lower boundaries touch each other at $k_x = 0$. When m drops below zero, the bulk gap reopens, the edge-state momentum windows for the two boundaries overlaps, and the edge states in the overlapping region enter the bulk gap. Interestingly, when m goes across zero, the edge states change *smoothly* according to Eqs. (2)–(5), although the system undergoes a *sudden* topological phase transition from the NI phase to the TI phase. In other words, the nontopological edge states in the NI phase and the topological edge states in the TI phase share the same physical origin and hence have many similarities. For example, when spin-down edge states are included by applying time reversal $k_x \to -k_x$ to Eqs. (2)–(5), the edge states in both the NI phase and the TI phase exhibit the same linear dispersion Eq. (2), spatial localization near the boundary of the QSHB, and helicity or spin-velocity locking. The helicity protects an edge state localized at one boundary of the QSHB from backscattering by nonmagnetic impurities to counterpropagating edge states localized at the same boundary. The spatial localization protects the edge states at one boundary from backscattering to counterpropagating edge states at the opposite boundary. The spatial separation of the edge states from the bulk states further reduces their scattering into the bulk states.

There does exist a key distinction between the edge states in the NI phase and those in the TI phase. The latter lie inside the gap of the bulk states and hence can be detected in transport measurements—the fingerprint of the TI phase. By contrast, the former usually lie outside the gap of the bulk states and overlap with the bulk states in the energy spectrum [e.g., see Figs. 2(c) and 2(d)]. This complicates their detection by transport measurements. Fortunately, two physical effects can separate the edge states from the bulk states in the energy spectrum and hence make the edge states detectable by transport measurements: (i) the quantum confinement effect by the finite width of the QSHB, to which the bulk states are sensitive but the edge states are not, and (ii) the presence of local electrostatic potential near the edge of the QSHB, to which the edge states are sensitive but the bulk states are not.

Nontopological edge states in the gap of bulk states. To capture the key physics of the local potential, which may arise either unintentionally in electrically gated samples or intentionally by using the side-gate technique [30–33], we consider a spatially dependent potential, which assumes a constant value V_U within 4 nm to the upper edge of the QSHB and a constant value V_L within 4 nm to the lower edge, and zero elsewhere, as shown in Fig. 3(a). To capture the quantum confinement effect, we consider a 200-nm-wide QSHB and calculate the energy spectrum by exact numerical diagonalization. In Fig. 3 we only show the spectrum of the spin-up states (that of the spin-down states is obtained by $k_x \to -k_x$) in the NI phase. As shown in Fig. 3(a), in the absence of any local potential, the edge states are already separated from the bulk states by ~4 meV due to the quantum confinement effect. Intuitively, applying a positive (negative) local potential at one boundary of the QSHB is expected to shift the edge states at this boundary upwards

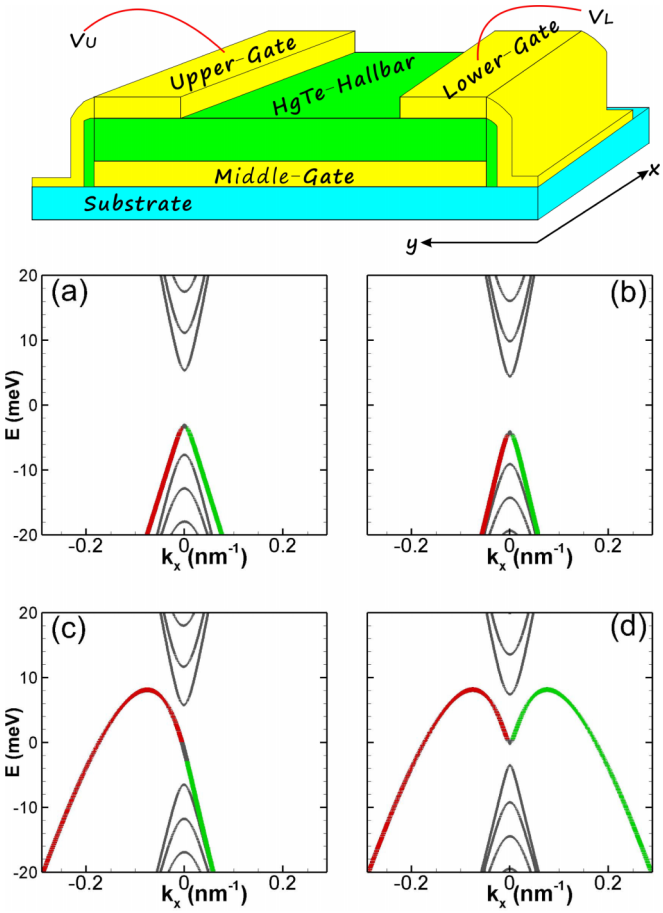

FIG. 3. The top panel sketches the side-gate setup capable of separating the nontopological edge states and the bulk states of the QSHB. The 200-nm-wide QSHB is embedded by two 4-nm-wide side gates. Each side gate produces a potential that is uniform underneath but zero elsewhere. The middle gate is grounded. Panels (a)–(d) show the spin-up energy spectra of the QSHB in the NI phase for different side-gate potentials: $V_U = V_L = 0$ for (a), $V_U = V_L = -80$ meV for (b), $V_U = -V_L = 80$ meV for (c), and $V_U = V_L = 80$ meV for (d). The gray lines are bulk states, and the green (red) lines are edge states at the lower (upper) boundary of the QSHB. The gap parameter $M = 2$ meV and other parameters are the same as Fig. 1, corresponding to $m \approx 0.04$. Since $\zeta > 0$, edge states appear in the highest valence band.

(downwards) but leaves other states largely intact. This expectation is confirmed by Figs. 3(b)–3(d). In Fig. 3(b), the negative local potential on both edges shifts all the edge states downwards. In Fig. 3(c), the positive local potential on the upper edge shifts the edge states at this edge upwards into the gap of the bulk states (and even makes the system gapless), and the negative local potential on the lower edge shifts the edge states at this edge downwards. In Fig. 3(d), the positive local potential on both edges shifts all edge states upwards into the gap of the bulk states, making the system gapless.

Once the nontopological edge states are separated from the bulk states, they become detectable by transport measurements when the Fermi level lies inside the gap of the bulk states. In particular, in the presence of positive local potential near both edges of the QSHB, i.e., Fig. 3(c), the Fermi level $E_F > 0$ has four intersections with the spin-up nontopological edge states, with two counterpropagating ones at each edge. Since the spectrum of the spin-down states is obtained from that of the spin-up states by $k_x \to -k_x$, the Fermi level also has four intersections with the spin-down nontopological edge states, with two counterpropagating ones at each edge. In other words, there are two spin-degenerate edge conductance channels inside the gap of the bulk states. Since the two counterpropagating spin-up (spin-down) edge states at the same edge can be scattered into each other by nonmagnetic disorder, the edge conductance is no longer quantized. In the NI phase of InAs/GaSb quantum wells, we obtain qualitatively the same behaviors (see the Supplemental Materials [39]). Therefore these nontopological edge states may offer a possible explanation for the puzzling experimental observation of two spin-degenerate, nonquantized conducting edge channels in the NI phase of InAs/GaSb quantum wells [14].

Conclusion. The topological insulator (TI) phase is a novel quantum state of the matter, featured by an insulator bulk and gapless edge modes at the boundary. For many years inversion of the bulk gap accompanied by the emergence of gapless and helical edge states at the boundary has been taken as a Hallmark of the 2D TI phase. Here we provide a "counterexample" by showing that the helical edge states emerge before band inversion as long as the bulk gap drops below a positive threshold determined by the degree of particle-hole asymmetry and the strength of the interband coupling. Since the k · p model describes a family of narrow-gap semiconductors with a strong interband coupling and the particle-hole asymmetry is ubiquitous in realistic materials, our work identifies a large class of narrow-gap semiconductor systems as platforms for edge-state physics. In the presence of a quantum confinement effect or local potentials near the edges of the sample, these nontopological edge states may be driven into the gap of the bulk states and be detected in transport measurements. This offers a possible solution to the puzzling experimental observation of conducting edge channels in the NI phase of InAs/GaSb quantum wells.

Acknowledgments. This work is supported by MOST of China (Grants No. 2017YFA0303400 and No. 2018YFA0306101), the National Natural Science Foundation of China (NSFC) (Grants No. 11974340, No. 11774021, and No. 61674145), the Chinese Academy of Sciences (Grants No. XDB28000000, No. QYZDJ-SSW-SYS001, and No. XXH13506-202), the NSAF grant in the NSFC with Grant No. U1930402. We acknowledge computational support from the Beijing Computational Science Research Center (CSRC).

[1] M. Z. Hasan and C. L. Kane, Rev. Mod. Phys. **82**, 3045 (2010).
[2] X.-L. Qi and S.-C. Zhang, Rev. Mod. Phys. **83**, 1057 (2011).
[3] C. L. Kane and E. J. Mele, Phys. Rev. Lett. **95**, 226801 (2005).
[4] C. L. Kane and E. J. Mele, Phys. Rev. Lett. **95**, 146802 (2005).

[5] B. A. Bernevig, T. L. Hughes, and S.-C. Zhang, Science **314**, 1757 (2006).

[6] M. Konig, S. Wiedmann, C. Brune, A. Roth, H. Buhmann, L. W. Molenkamp, X.-L. Qi, and S.-C. Zhang, Science **318**, 766 (2007).

[7] X.-L. Qi, T. L. Hughes, and S.-C. Zhang, Phys. Rev. B **78**, 195424 (2008).

[8] C. Liu, T. L. Hughes, X.-L. Qi, K. Wang, and S.-C. Zhang, Phys. Rev. Lett. **100**, 236601 (2008).

[9] I. Knez, R.-R. Du, and G. Sullivan, Phys. Rev. Lett. **107**, 136603 (2011).

[10] B. Zhou, H.-Z. Lu, R.-L. Chu, S.-Q. Shen, and Q. Niu, Phys. Rev. Lett. **101**, 246807 (2008).

[11] M. König, H. Buhmann, L. W. Molenkamp, T. Hughes, C.-X. Liu, X.-L. Qi, and S.-C. Zhang, J. Phys. Soc. Jpn. **77**, 031007 (2008).

[12] M. S. Miao, Q. Yan, C. G. Van de Walle, W. K. Lou, L. L. Li, and K. Chang, Phys. Rev. Lett. **109**, 186803 (2012).

[13] D. Zhang, W. Lou, M. Miao, S.-c. Zhang, and K. Chang, Phys. Rev. Lett. **111**, 156402 (2013).

[14] F. Nichele, H. J. Suominen, M. Kjaergaard, C. M. Marcus, E. Sajadi, J. A. Folk, F. Qu, A. J. A. Beukman, F. K. de Vries, J. van Veen, S. Nadj-Perge, L. P. Kouwenhoven, B.-M. Nguyen, A. A. Kiselev, W. Yi, M. Sokolich, M. J. Manfra, E. M. Spanton, and K. A. Moler, New J. Phys. **18**, 083005 (2016).

[15] E. Y. Ma, M. R. Calvo, J. Wang, B. Lian, M. Mühlbauer, C. Brüne, Y.-T. Cui, K. Lai, W. Kundhikanjana, Y. Yang, M. Baenninger, M. König, C. Ames, H. Buhmann, P. Leubner, L. W. Molenkamp, S.-C. Zhang, D. Goldhaber-Gordon, M. A. Kelly, and Z.-X. Shen, Nat. Commun. **6**, 7252 (2015).

[16] L. Du, I. Knez, G. Sullivan, and R.-R. Du, Phys. Rev. Lett. **114**, 096802 (2015).

[17] S. Mueller, A. N. Pal, M. Karalic, T. Tschirky, C. Charpentier, W. Wegscheider, K. Ensslin, and T. Ihn, Phys. Rev. B **92**, 081303(R) (2015).

[18] D. I. Pikulin and T. Hyart, Phys. Rev. Lett. **112**, 176403 (2014).

[19] R. W. Reinthaler and E. M. Hankiewicz, Phys. Rev. B **85**, 165450 (2012).

[20] G. Tkachov and E. M. Hankiewicz, Phys. Rev. Lett. **104**, 166803 (2010).

[21] L.-H. Hu, D.-H. Xu, F.-C. Zhang, and Y. Zhou, Phys. Rev. B **94**, 085306 (2016).

[22] M. Karalic, S. Mueller, C. Mittag, K. Pakrouski, Q. S. Wu, A. A. Soluyanov, M. Troyer, T. Tschirky, W. Wegscheider, K. Ensslin, and T. Ihn, Phys. Rev. B **94**, 241402(R) (2016).

[23] L.-H. Hu, C.-C. Chen, C.-X. Liu, F.-C. Zhang, and Y. Zhou, Phys. Rev. B **96**, 075130 (2017).

[24] L. Du, X. Li, W. Lou, G. Sullivan, K. Chang, J. Kono, and R.-R. Du, Nat. Commun. **8**, 1971 (2017).

[25] S. Mueller, C. Mittag, T. Tschirky, C. Charpentier, W. Wegscheider, K. Ensslin, and T. Ihn, Phys. Rev. B **96**, 075406 (2017).

[26] C.-A. Li, S.-B. Zhang, and S.-Q. Shen, Phys. Rev. B **97**, 045420 (2018).

[27] R. Skolasinski, D. I. Pikulin, J. Alicea, and M. Wimmer, Phys. Rev. B **98**, 201404(R) (2018).

[28] D. R. Candido, M. E. Flatté, and J. C. Egues, Phys. Rev. Lett. **121**, 256804 (2018).

[29] R. Winkler, *Spin-Orbit Coupling Effects in Two-Dimensional Electron and Hole Systems* (Springer, Berlin, 2003).

[30] P. M. Campbell, E. S. Snow, and P. J. McMarr, Appl. Phys. Lett. **66**, 1388 (1995).

[31] D. Stornaiuolo, S. Gariglio, A. Fête, M. Gabay, D. Li, D. Massarotti, and J.-M. Triscone, Phys. Rev. B **90**, 235426 (2014).

[32] A. M. R. V. L. Monteiro, D. J. Groenendijk, N. Manca, E. Mulazimoglu, S. Goswami, Y. Blanter, L. M. K. Vandersypen, and A. D. Caviglia, Nano Lett. **17**, 715 (2017).

[33] Z. Lei, C. A. Lehner, E. Cheah, C. Mittag, M. Karalic, W. Wegscheider, K. Ensslin, and T. Ihn, Phys. Rev. Research **3**, 023042 (2021).

[34] B. Buttner, C. X. Liu, G. Tkachov, E. G. Novik, C. Brune, H. Buhmann, E. M. Hankiewicz, P. Recher, B. Trauzettel, S. C. Zhang, and L. W. Molenkamp, Nat. Phys. **7**, 418 (2011).

[35] C. Brüne, C. Thienel, M. Stuiber, J. Böttcher, H. Buhmann, E. G. Novik, C.-X. Liu, E. M. Hankiewicz, and L. W. Molenkamp, Phys. Rev. X **4**, 041045 (2014).

[36] I. Knez, R.-R. Du, and G. Sullivan, Phys. Rev. Lett. **109**, 186603 (2012).

[37] K. Suzuki, Y. Harada, K. Onomitsu, and K. Muraki, Phys. Rev. B **87**, 235311 (2013).

[38] I. Knez, C. T. Rettner, S.-H. Yang, S. S. P. Parkin, L. Du, R.-R. Du, and G. Sullivan, Phys. Rev. Lett. **112**, 026602 (2014).

[39] See Supplemental Material at http://link.aps.org/supplemental/10.1103/PhysRevB.105.045305 for more detail in reducing the effective Hamiltonian. The Supplemental Material include the following: (1) detailed reduced derivation of effective Hamiltonian with four bands and eight bands; (2) numerical calculation results of effective Hamiltonian with eight bands; (3) detailed analytical derivation and numerical results of four bands effective Hamiltonian; and (4) the effective four-band Hamiltonian parameters of common narrow-band-gap semiconductors.

[40] M. G. Burt, J. Condens. Matter Phys. **4**, 6651 (1992).

[41] L. Per-Olov, J. Chem. Phys. **19**, 1396 (1951).

[42] I. Vurgaftman, J. R. Meyer, and L. R. Ram-Mohan, J. Appl. Phys. **89**, 5815 (2001).

[43] J. Li, W. Yang, and K. Chang, Phys. Rev. B **80**, 035303 (2009).

[44] Y. R. Lin-Liu and L. J. Sham, Phys. Rev. B **32**, 5561 (1985).

[45] L. B. Zhang, F. Cheng, F. Zhai, and K. Chang, Phys. Rev. B **83**, 081402(R) (2011).

[46] T. Ando, A. B. Fowler, and F. Stern, Rev. Mod. Phys. **54**, 437 (1982).

[47] M. A. Tito, Y. A. Pusep, A. Gold, M. D. Teodoro, G. E. Marques, and R. R. LaPierre, J. Appl. Phys. **119**, 094301 (2016).

[48] Z. Lei, C. A. Lehner, K. Rubi, E. Cheah, M. Karalic, C. Mittag, L. Alt, J. Scharnetzky, P. Märki, U. Zeitler, W. Wegscheider, T. Ihn, and K. Ensslin, Phys. Rev. Research **2**, 033213 (2020).

[49] C.-Z. Ning, L. Dou, and P. Yang, Nat. Rev. Mater. **2**, 17070 (2017).

[50] J. Li, C. Tang, P. Du, Y. Jiang, Y. Zhang, X. Zhao, Q. Gong, and X. Kou, Appl. Phys. Lett. **116**, 122102 (2020).

[51] G. Tuttle, H. Kroemer, and J. H. English, J. Appl. Phys. **65**, 5239 (1989).

[52] J. L. Jimenez, X. Li, and W. I. Wang, Appl. Phys. Lett. **64**, 2127 (1994).

[53] E. E. Mendez, W. I. Wang, B. Ricco, and L. Esaki, Appl. Phys. Lett. **47**, 415 (1985).

[54] P. Chen, W. V. Chen, P. K. L. Yu, C. W. Tang, K. M. Lau, L. Mawst, C. Paulson, T. F. Kuech, and S. S. Lau, Appl. Phys. Lett. **94**, 012101 (2009).

[55] M. Karalic, C. Mittag, M. Hug, T. Tschirky, W. Wegscheider, K. Ensslin, T. Ihn, K. Shibata, and R. Winkler, Phys. Rev. B **99**, 115435 (2019).

[56] L. V. Ginzburg, C. Gold, M. P. Roosli, C. Reichl, M. Berl, W. Wegscheider, T. Ihn, and K. Ensslin, Phys. Rev. Research **3**, 023033 (2021).